Atmospheric
Chemistry
and Physics

Supplement of

Daytime isoprene nitrates under changing NO$_x$ and O$_3$

Alfred W. Mayhew et al.

Correspondence to: Jaqueline F. Hamilton (jacqui.hamilton@york.ac.uk)
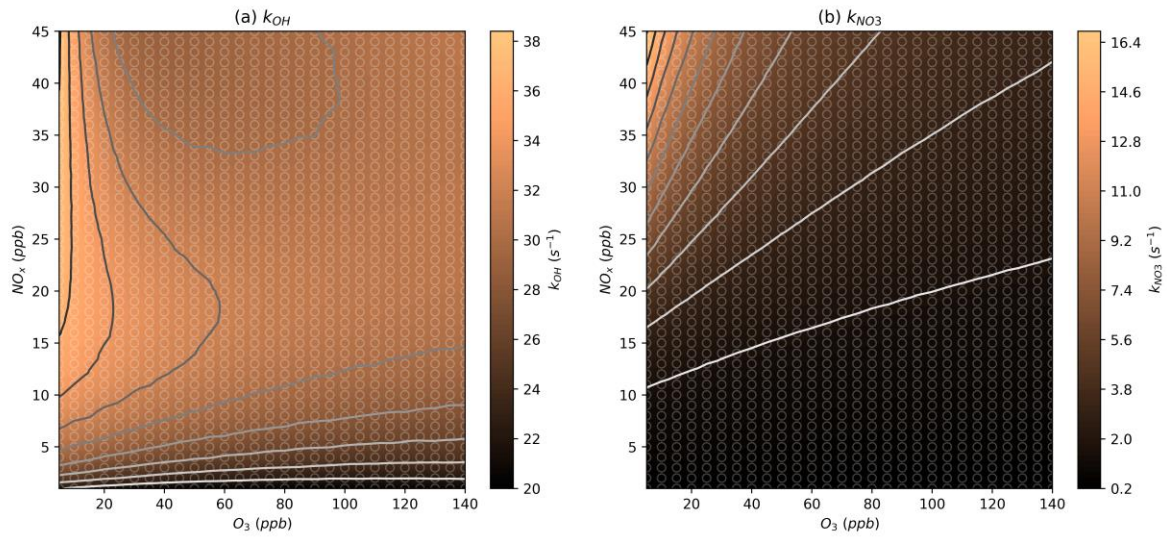
Section S1 - Model Validation Plots

Figure S1. Modelled steady-state k_{OH} and k_{NO3} values at a wider range of NO_x and O_3 mixing ratios.
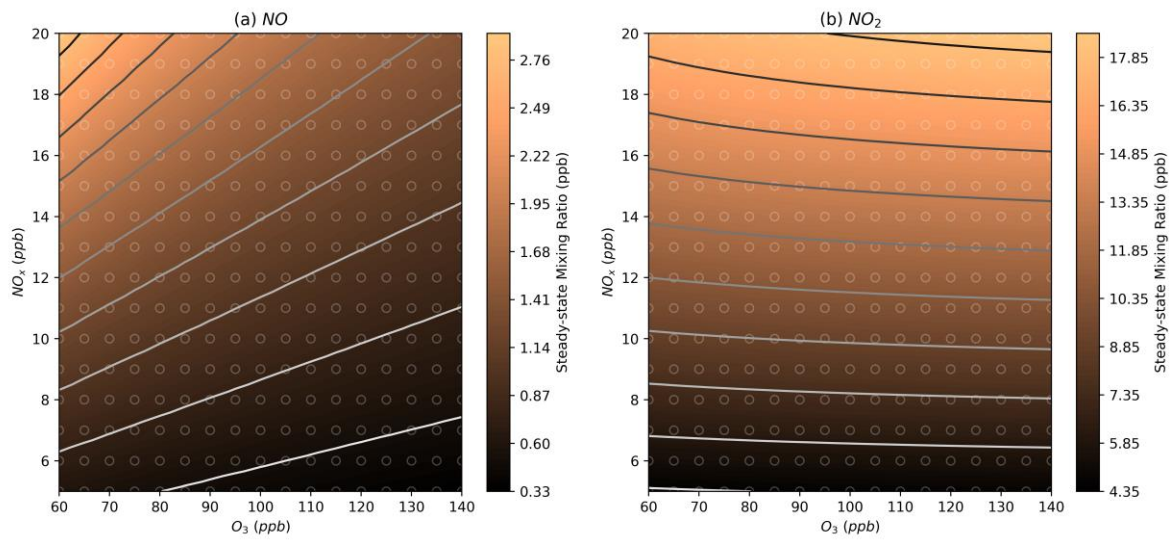

Figure S2. Modelled steady-state mixing ratios of NO and NO_2 at NO_x and O_3 mixing ratios representative of those observed during the Beijing 2017 campaign.
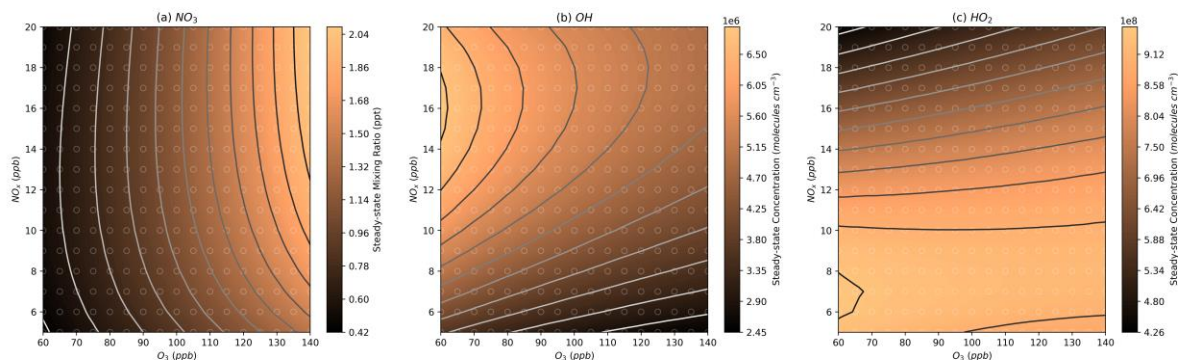
Figure S3. Modelled steady-state concentrations of NO₃, OH, and HO₂ at NOₓ and O₃ mixing ratios representative of those observed during the Beijing 2017 campaign.

Section S2 - Sensitivity Tests

Figure S5 and Figure S6 show the isopleths for each organonitrate group investigated in this work under a lower isoprene mixing ratio of 0.5 ppb and a higher isoprene mixing ratio of 3 ppb. Increasing the isoprene mixing ratio has three effects: the absolute concentration of isoprene oxidation products increases for a given model run; the peak concentrations of IHN and other OH-initiated products occurs under higher NO_x conditions; the transition from NO_x-sensitive to O_3-sensitive regions in NO_3-initiated species occurs more gradually over a broader range of NO_x mixing ratios. These effects are explained later in this section. The shape of the isopleths, and hence the conclusions drawn regarding changes in O_3 and NO_x concentrations, are consistent despite changing isoprene concentrations, and a discussion of the impact of changing isoprene concentrations on organonitrate concentrations will be included where necessary throughout the paper.

Methane was added to the model in order to account for additional reactivity which would be provided by other VOCs under ambient conditions. The mixing ratio of methane in the models was halved and doubled in two tests (41 ppm and 164 ppm respectively), and the results are shown in Figure S7 and Figure S8. The effect of increasing methane in the models on the shape of the concentration profiles is similar to the effect of increasing isoprene concentrations, though the absolute peak concentrations of the isoprene oxidation products does not change significantly. Higher methane concentrations result in the peak concentrations of OH-initiated products occurring at higher NO_x mixing ratios and also the broadening of the transition between NO_x-sensitive and O_3-sensitive regions in NO_3-initiated products.

For OH, the higher VOC concentrations mean that more NO_x is required to produce the same amount of OH at a given O_3 to compensate for the increased conversion of OH to HO_2 (Figure S4).

Similarly, for a given pair of O_3 and NO_x concentrations, the NO_3 concentrations will be higher at a higher NO_2/NO ratio due to higher formation from the NO_2+O_3 reaction as well as lower loss from the NO_3+NO reaction. In these models, the NO_2/NO ratio is largely dictated by HO_2 and O_3 concentrations. Since O_3 is held constant and HO_2 concentrations are low at high NO_x concentrations (Figure 6c), the NO_2/NO ratio is constant for a given O_3 concentration at high NO_x (Figure S9). There is an increase in NO_2 at low-NO_x where HO_2 concentrations are important for converting NO to NO_2. The NO_3 profile corresponds to this NO_2/NO ratio profile, with the added decrease in NO_3 concentrations at low NO_x due to the availability of NO_2 for NO_3 formation (Figure 6a). Therefore, when HO_2 concentrations increase due to higher VOC concentrations, the NO_2/NO ratio will increase allowing greater concentrations of NO_3.
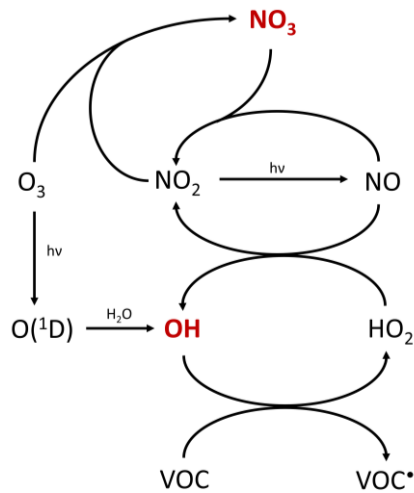
Figure S4. The chemical cycles controlling NO_3 and OH. Some reaction pathways have been omitted for clarity.
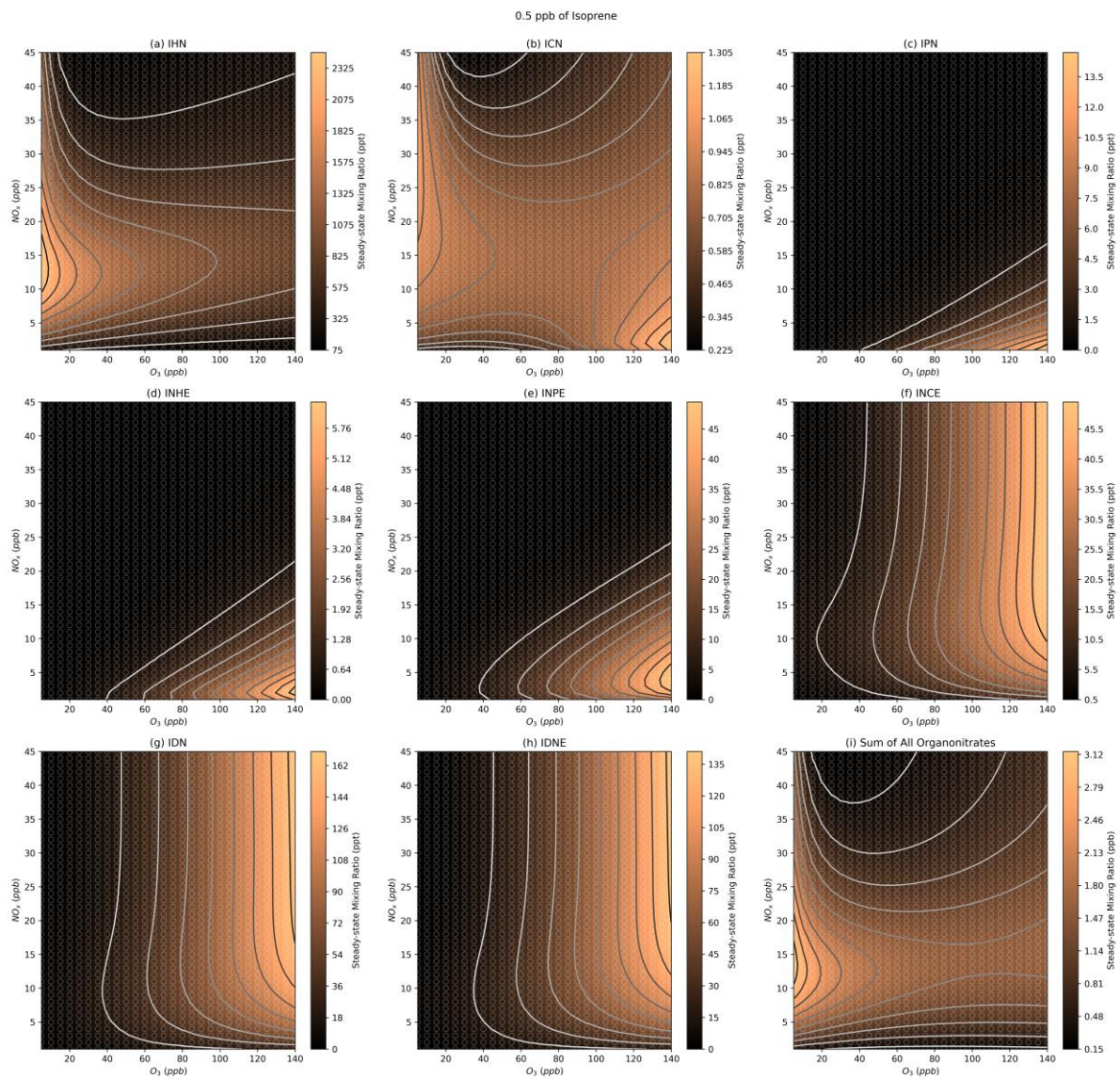

Figure S5. Modelled steady state organonitrate concentrations at the lower isoprene mixing ratio of 0.5 ppb.
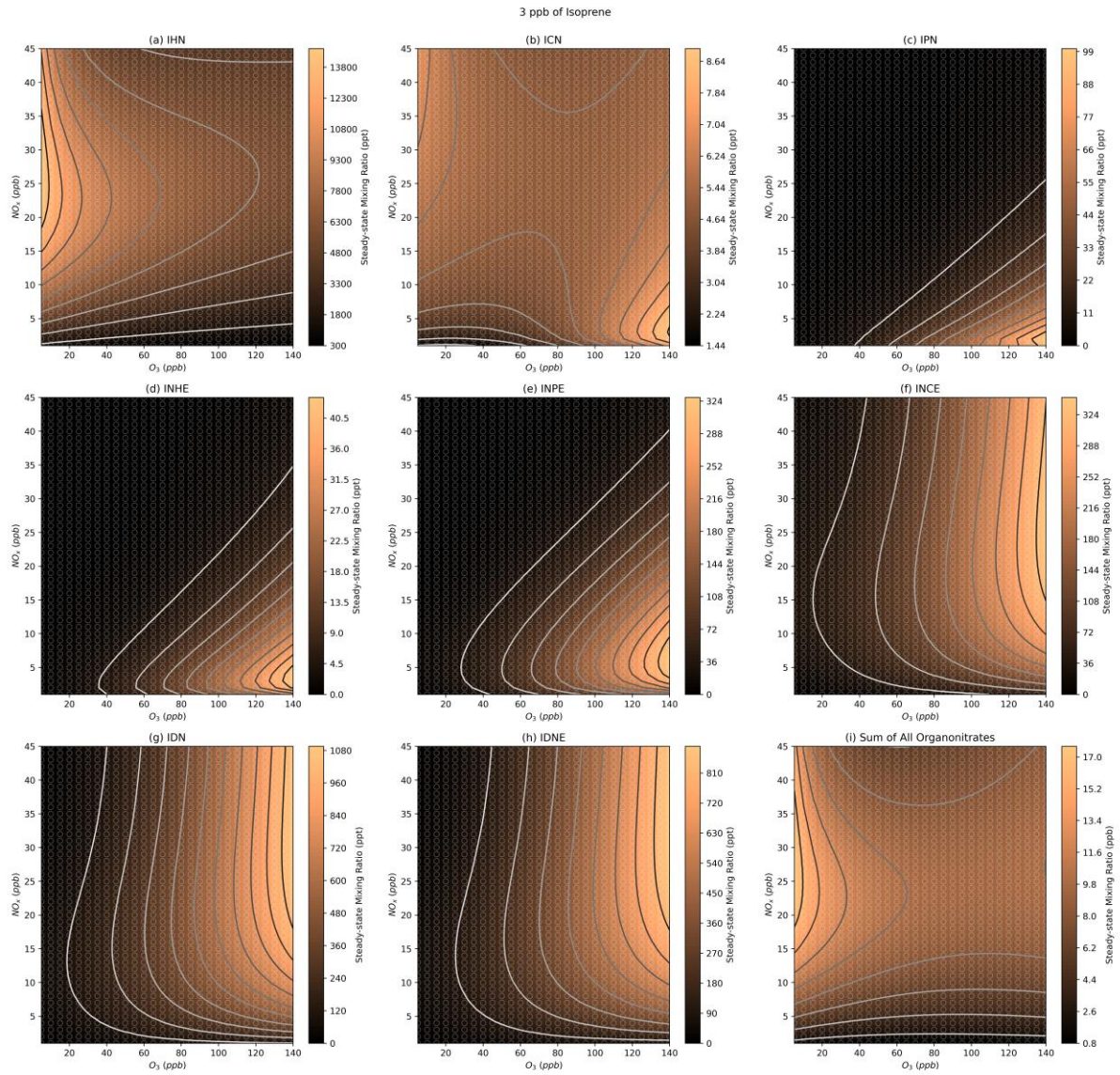
Figure S6. Modelled steady state organonitrate concentrations at the higher isoprene mixing ratio of 3 ppb.
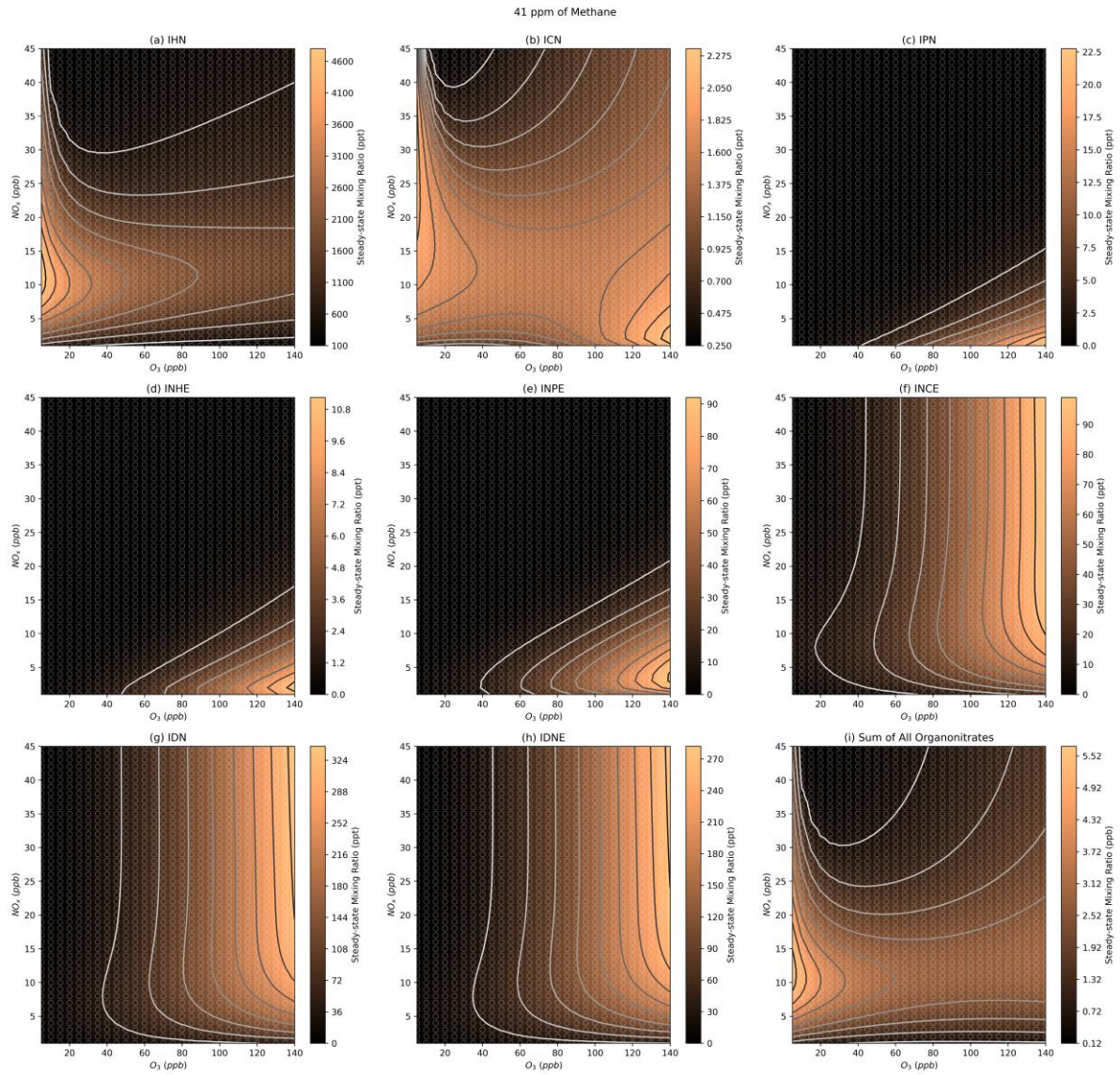
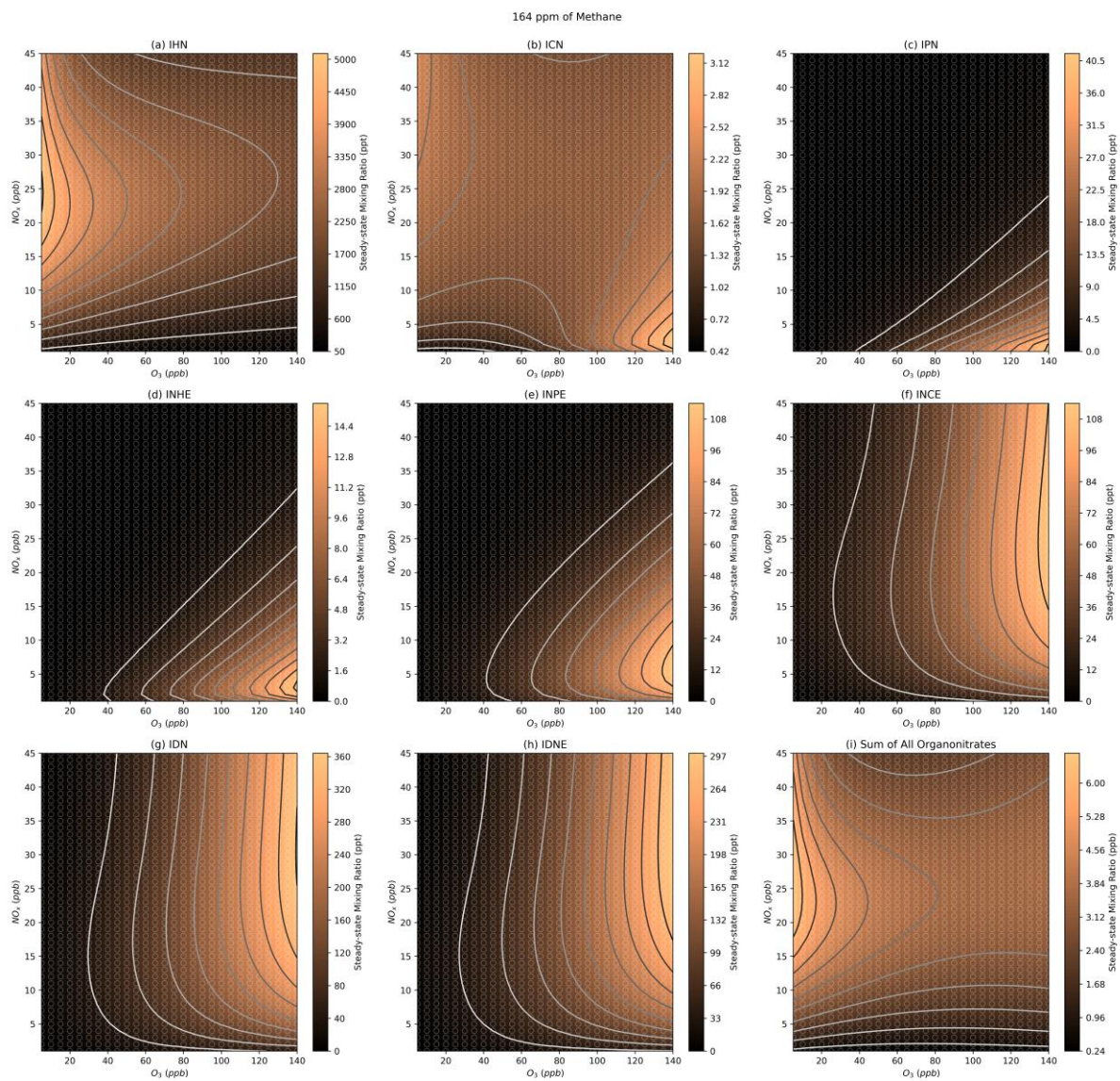*Figure S7. Modelled steady state organonitrate concentrations at the lower methane mixing ratio of 41 ppm.*

Figure S8. Modelled steady state organonitrate concentrations at the higher methane mixing ratio of 164 ppm.
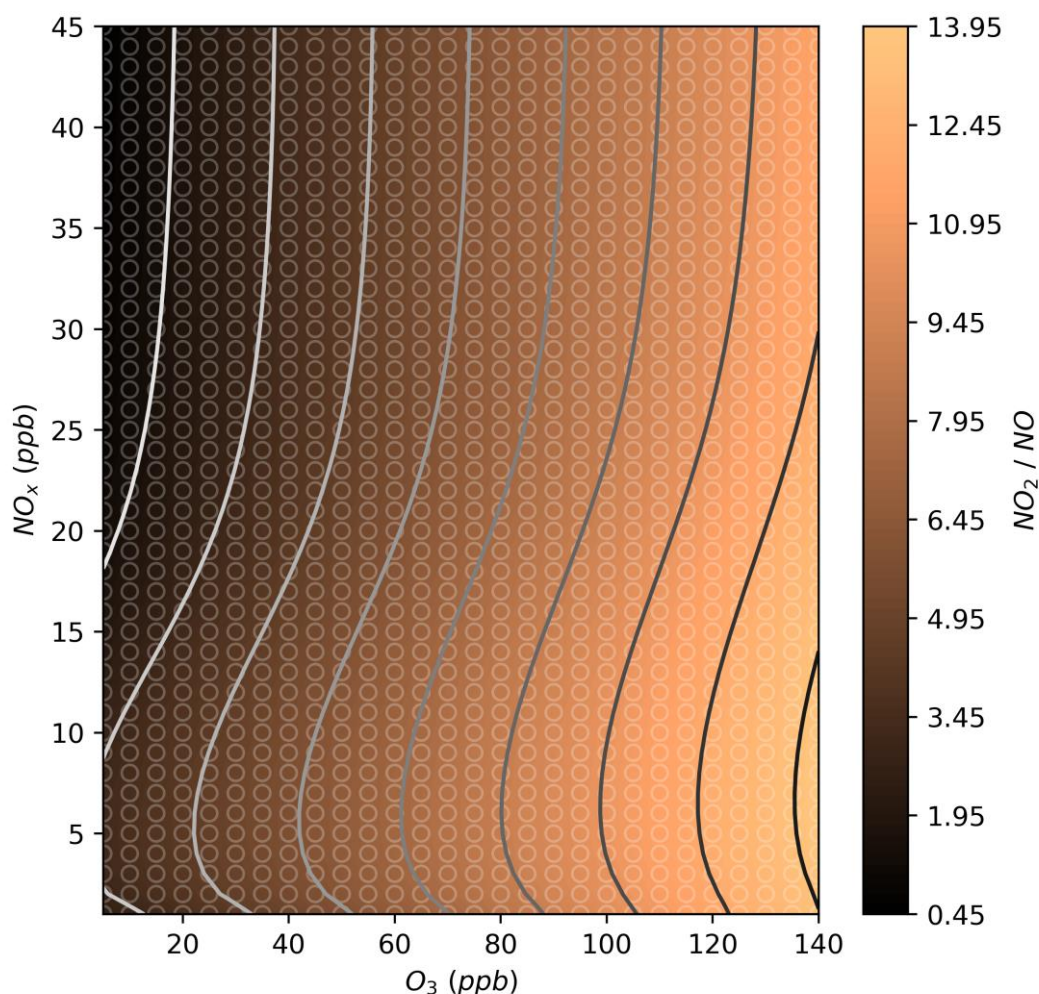
Figure S9. Modelled steady-state NO$_2$/NO ratios at a range of NO$_x$ and O$_3$ mixing ratios.

The dilution rate included in the models of 2.31×10^{-5} s^{-1} was chosen to give a lifetime with respect to dilution of 12 hours. To test the sensitivity of the results to this decision, additional models were run with dilution lifetimes of 1 hour, 6 hours, and 24 hours. When halving the dilution rate such that the lifetime with respect to dilution is 24 hours (Figure S10), the absolute concentrations of the organonitrates increase due to the reduction in losses. However, the profile of the isopleths does not change. Similarly, doubling the dilution rate decreases species concentrations but does not alter the isopleth profiles (Figure S11). Increasing the dilution rate further, resulting in a dilution lifetime of 1 hour, does skew the isopleth profiles compared to the longer lifetime models, particularly impacting OH and OH-initiated products like IHN (Figure S12). Despite the difference made by this extreme change, many of the conclusions made in this work would hold true with regards to the NO$_x$-O$_3$ regimes favoured by different organonitrate groups.
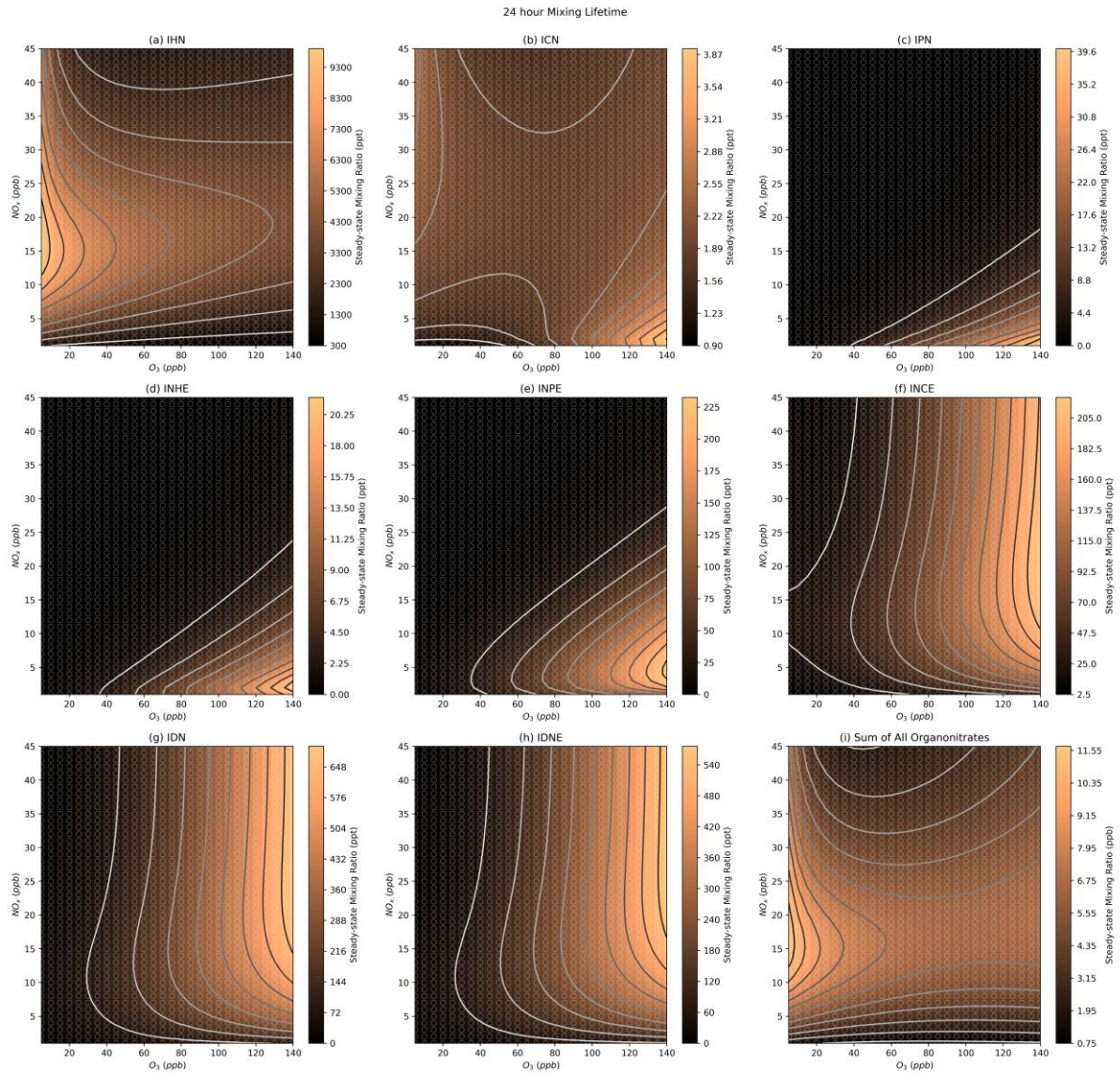
Figure S10. Modelled steady state organonitrate concentrations at the longer dilution lifetime of 24 hours.
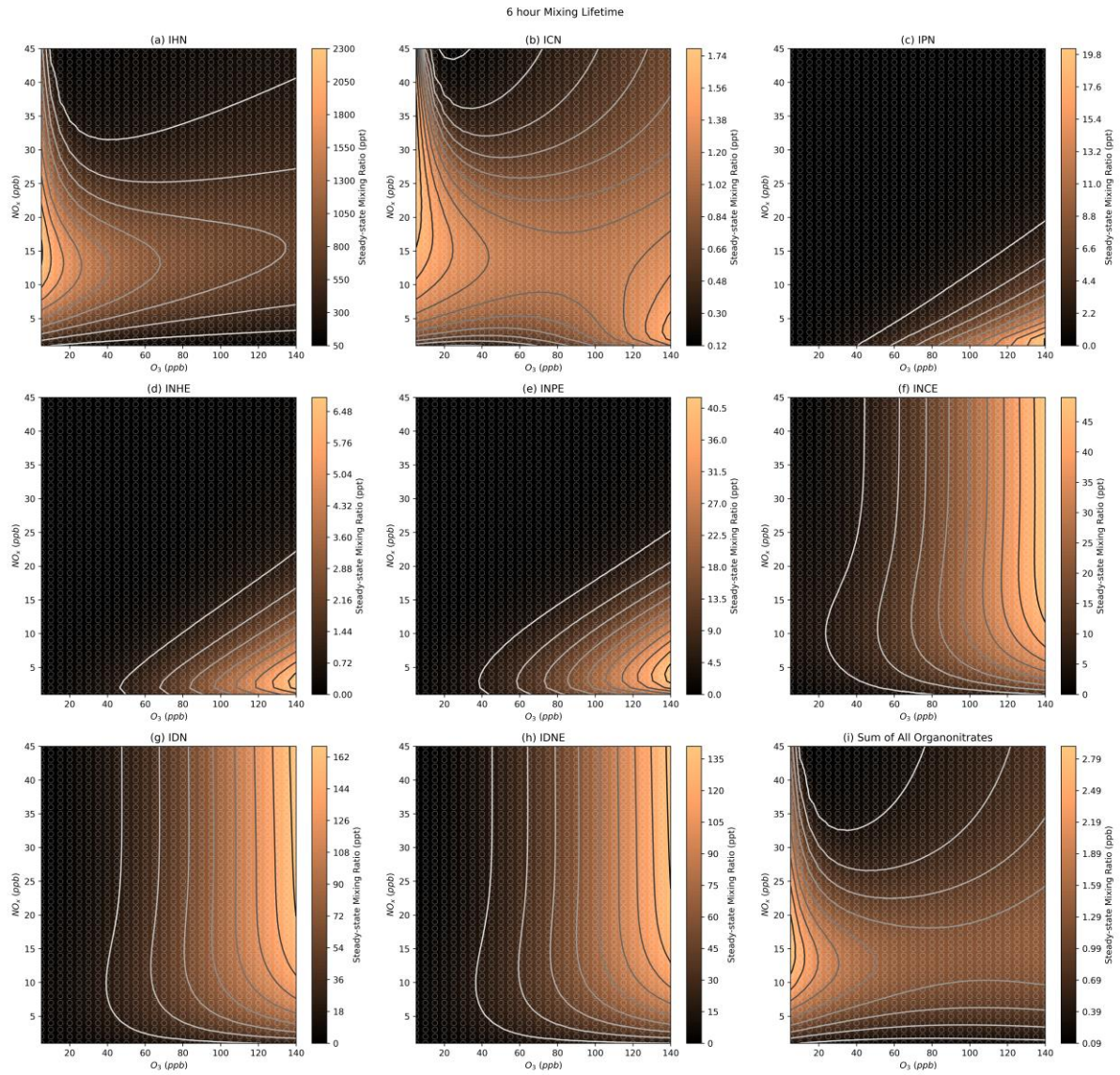
Figure S11. Modelled steady state organonitrate concentrations at the shorter dilution lifetime of 6 hours.
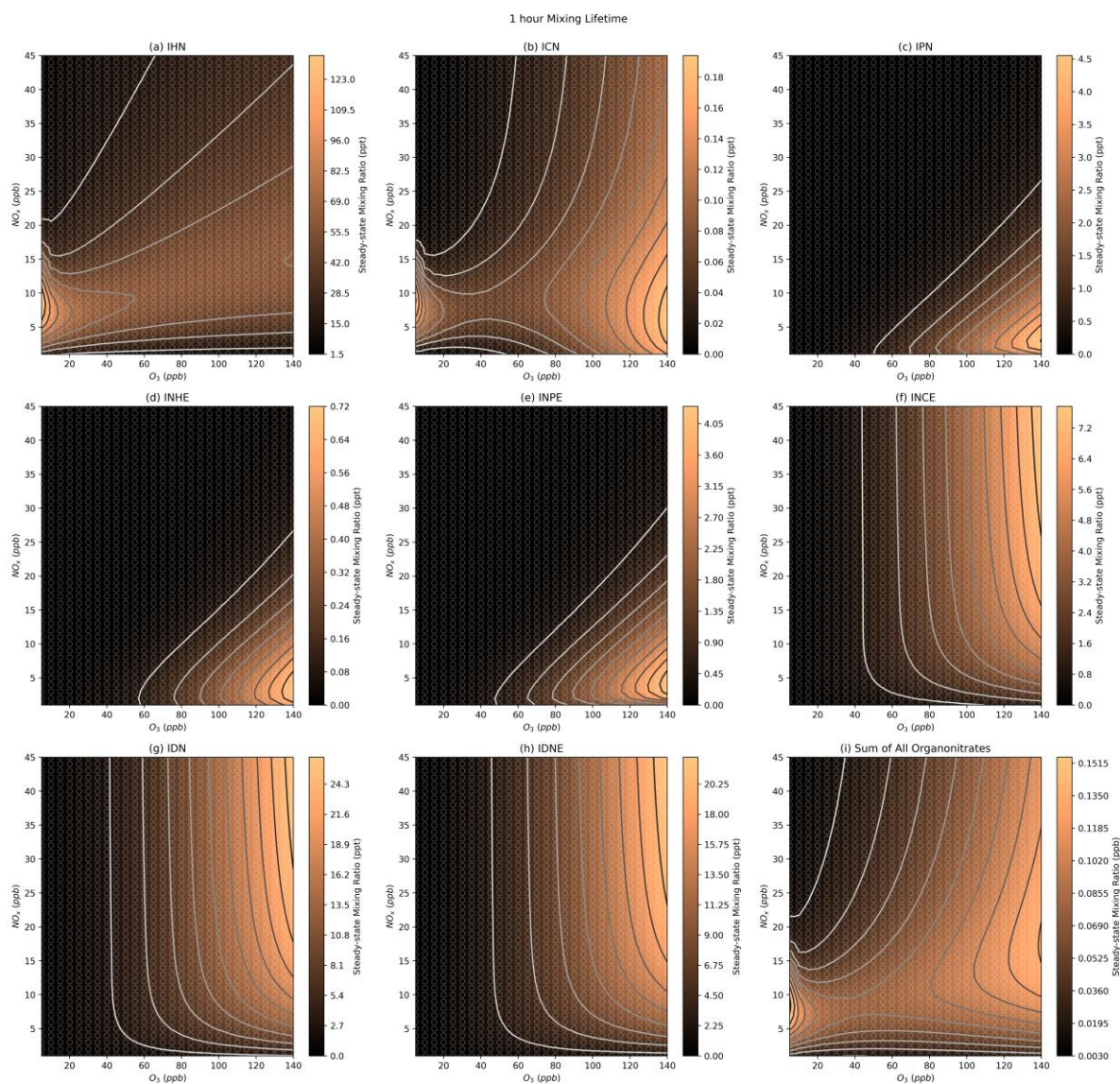
Figure S12. Modelled steady state organonitrate concentrations at the shorter dilution lifetime of 1 hour.

Although these models focus on the afternoon-period in Beijing, two separate sets of models were run under differing photolysis conditions corresponding to different times in the afternoon in Beijing, 2 hours before and after the chosen time of 16:00 local time (Figure S13 and Figure S14). The earlier time of 14:00 results in higher absolute concentrations of OH-initiated species such as IHN and slightly lower absolute concentrations of NO_3 initiated species as a result of increased NO_3 photolysis and higher NO concentrations. Despite the absolute differences in concentration, the profile of the NO_x-O_3 isopleth for each organonitrate group does not change significantly, though the impact of the NO_3-initiated organonitrates at high O_3 mixing ratios in the total organonitrate isopleth is lessened. The later time of 18:00 is entering dusk in the summer of Beijing, so the role of NO_3 chemistry is amplified and the OH chemistry is reduced. This is clear from the IHN profile which shows that the peak concentration occurs at high O_3 and NO_x, since the NO_3-initiated pathway becomes the dominant formation route. This change means that the total organonitrate isopleth shape is very different in the 18:00 model, with the highest concentrations occurring under high-O_3-high-NO_x conditions, where NO_3 is the highest. These time-of-day sensitivity tests illustrate that the conclusions made in this work are applicable during daytime photolysis conditions.
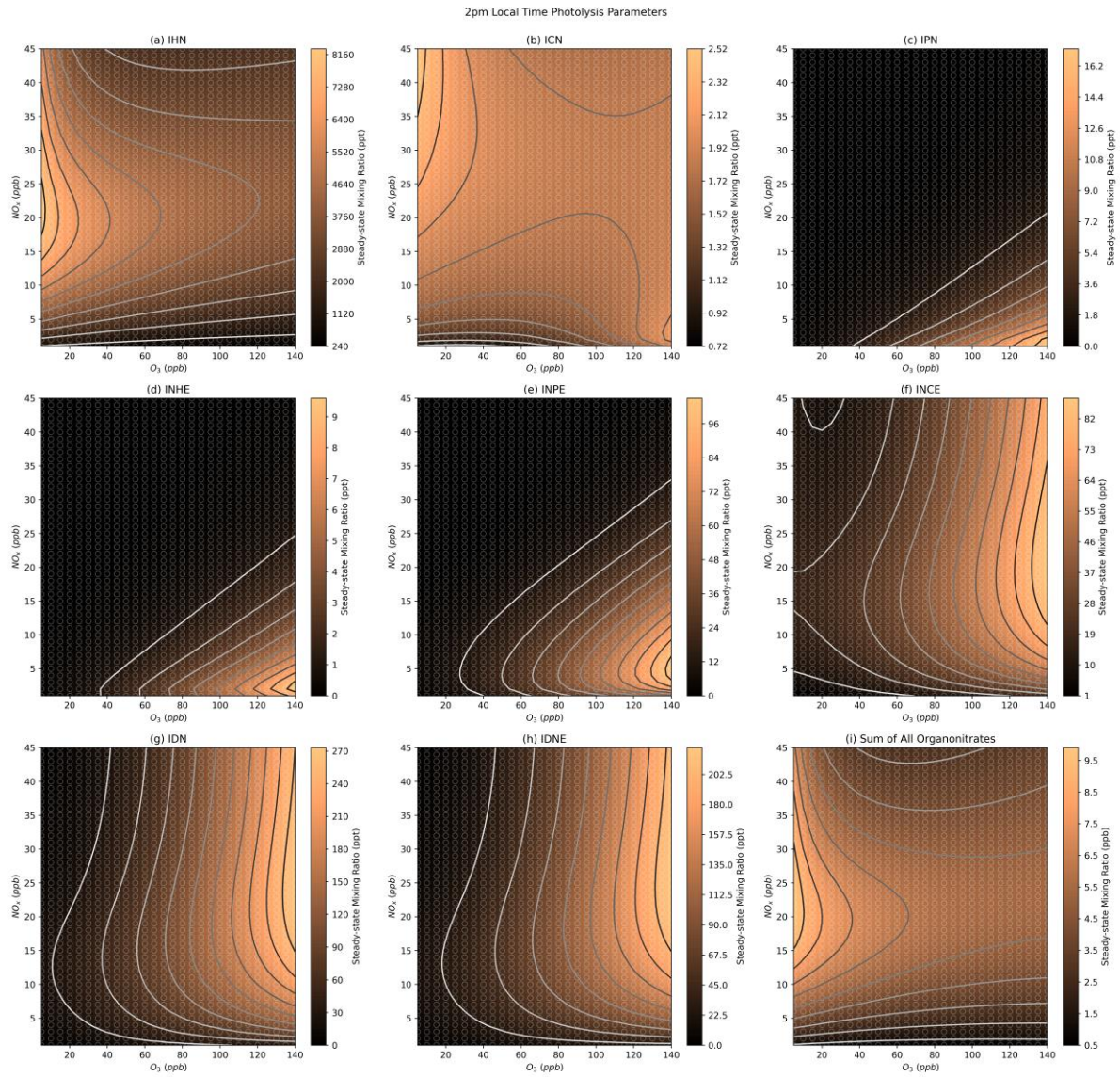
Figure S13. Modelled steady state organonitrate concentrations with photolysis conditions corresponding to the earlier model time of 14:00 local time.
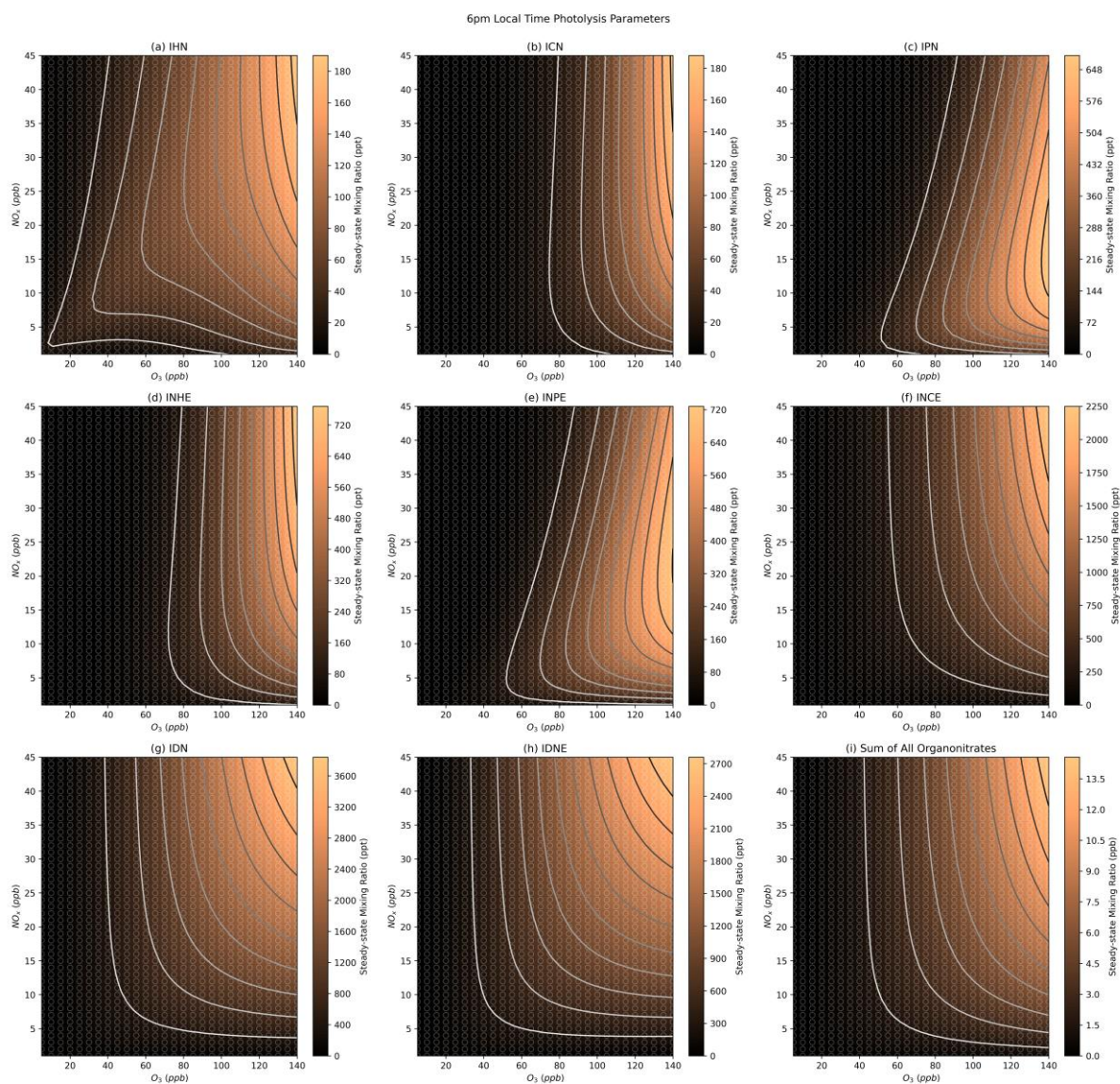
Figure S14. Modelled steady state organonitrate concentrations with photolysis conditions corresponding to the later model time of 18:00 local time.

Section S3 - Saturation Concentration

As an alternative to the compound vapour pressures used in Section 4.6 of the main text, the saturation concentration (expressed as a log value, $\log_{10}(C_{Sat})$)) was estimated in order to assess the impact of changes in NO_x and O_3 on SOA. The method for estimating $\log_{10}(C_{Sat})$ is taken from Mohr *et al.* 2019, and uses Equation 1 to estimate $\log_{10}(C_{Sat})$ based on the molecular formula of each compound. n_C, n_N, and n_O are the number of carbon, nitrogen, and oxygen atoms respectively. b_C, b_O, b_{CO} and b_N are 0.475, 0.2, 0.9, 2.5 respectively. (Mohr et al., 2019; Donahue et al., 2011)

$$\log_{10}(S_{sat}) = (25 - n_C)b_C - (n_O - 3n_N)b_O - 2\frac{(n_O - 3n_N)\,n_C}{n_C + n_O - 3n_N}b_{CO} - n_N b_N \qquad Equation\ 1$$

This method does not account for the structure of each individual compound, hence the use of UManSysProp in the main text, but is presented here as an alternative method due to the different profile in Figure S15 compared to Figure 13. Figure S15 shows two peaks in normalised

concentration, one at low O_3 and one at high O_3, in a similar fashion to the total organonitrate plot in Figure 12. However, due to the lower volatilities of the species formed under high O_3, the two normalised concentration peaks are of a similar magnitude in Figure S15. This means that, depending on the initial position in NO_x-O_3 space, reductions in either NO_x or O_3 may result in increases in organonitrate SOA.
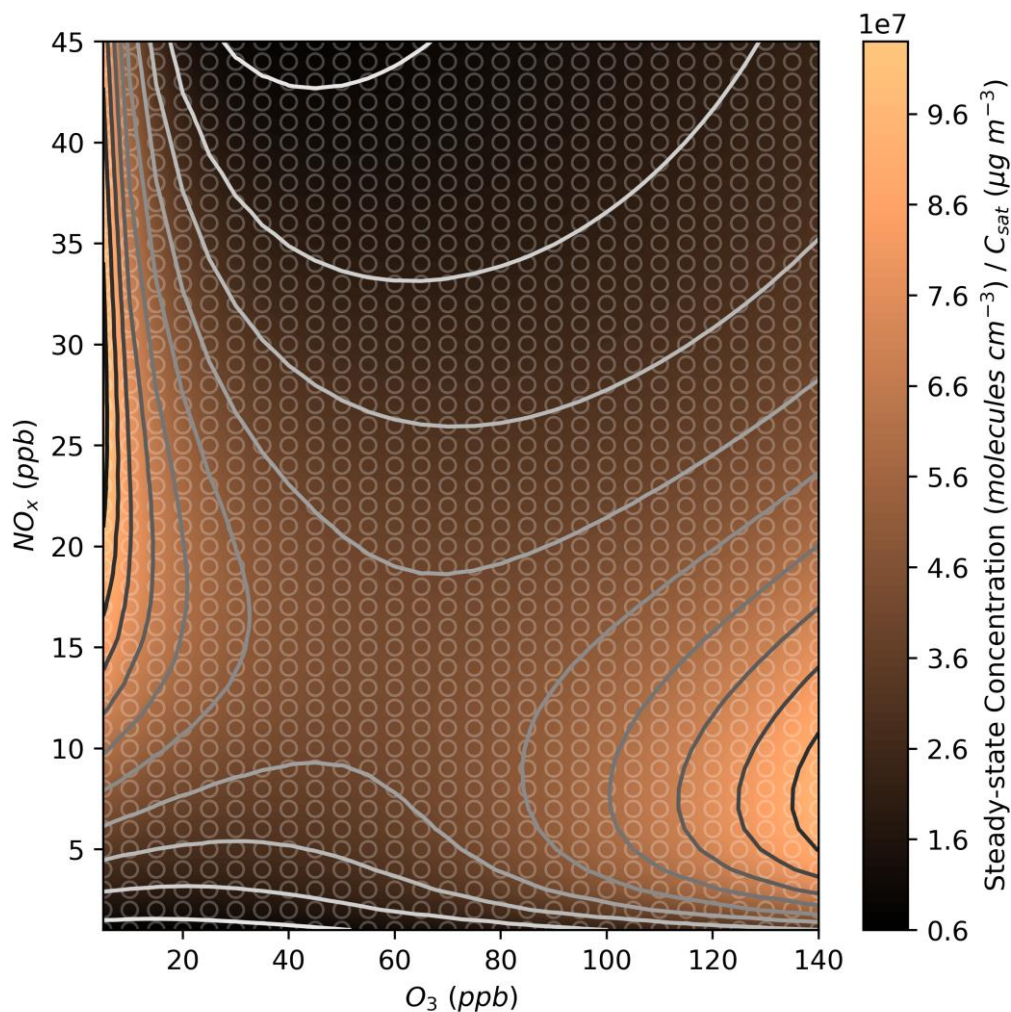

Figure S15. Modelled steady-state concentrations of the total organonitrates normalised to each compound's estimated saturation concentration at different NO_x and O_3 mixing ratios.

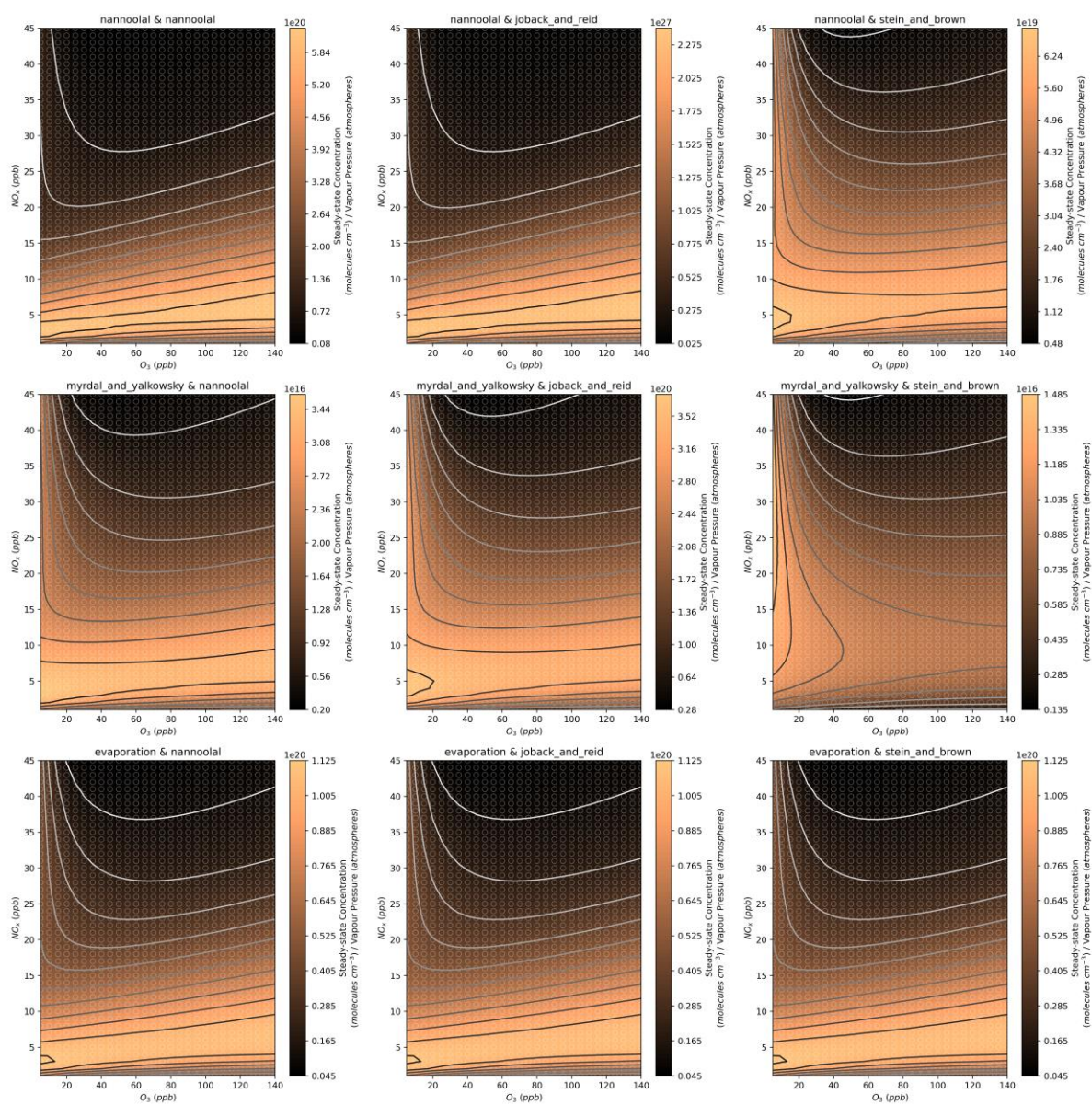# Section S4 - Additional Vapour Pressure Plots

Figure S16. Modelled steady-state concentrations of the total organonitrates normalised to each compound's estimated vapour pressure at different NO$_x$ and O$_3$ mixing ratios using each combination of vapour pressure and boiling point methods available through the UManSysProp API.
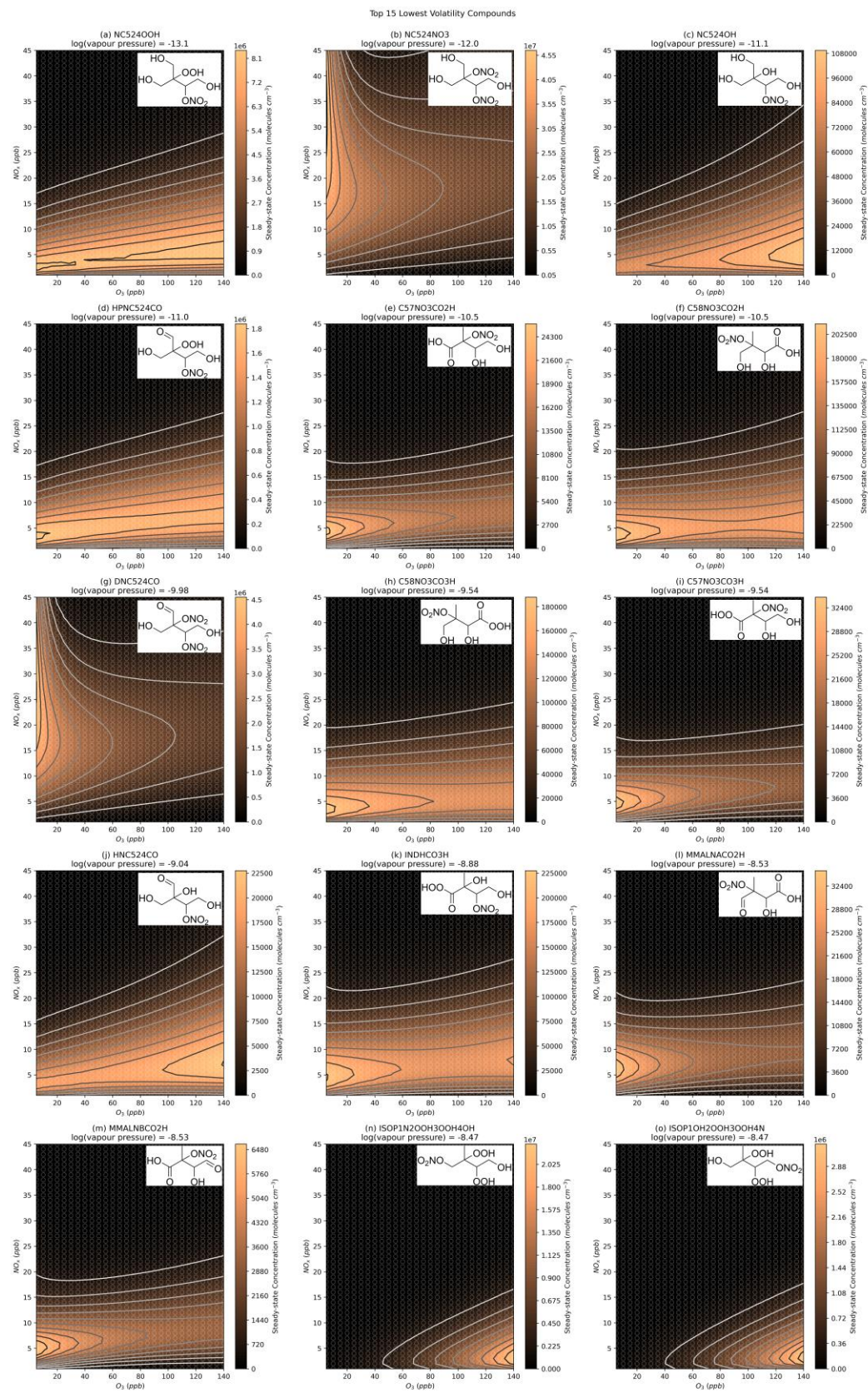
Figure S17. Modelled steady state concentrations of the 15 lowest volatility compounds at different NO$_x$ and O$_3$ mixing ratios.
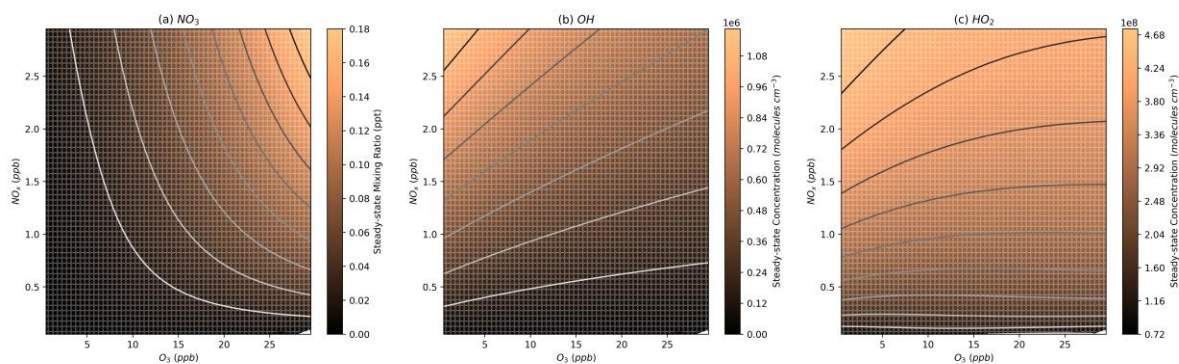
Section S5 - Amazon Models

Figure S18. Modelled steady-state concentrations of NO₃, OH, and HO₂ in the Amazon models (lower NOₓ and O₃ concentrations and higher VOC concentrations than the Beijing models).
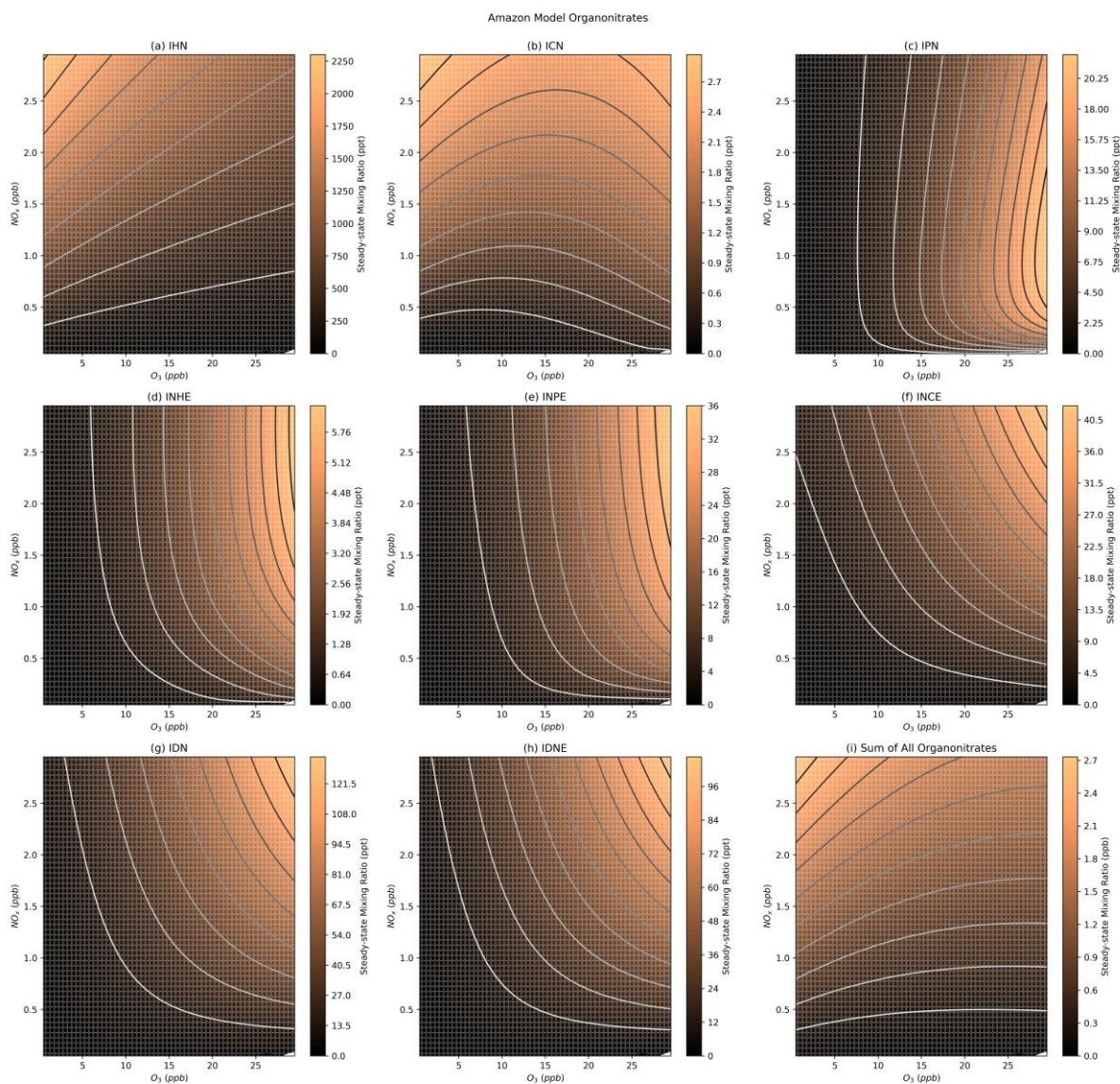

Figure S19. Modelled steady state organonitrate concentrations for the Amazon models (lower NOₓ and O₃ concentrations and higher VOC concentrations than the Beijing models).

References

Donahue, N. M., Epstein, S. A., Pandis, S. N., and Robinson, A. L.: A two-dimensional volatility basis set: 1. organic-aerosol mixing thermodynamics, Atmospheric Chemistry and Physics, 11, 3303-3318, 10.5194/acp-11-3303-2011, 2011.

Mohr, C., Thornton, J. A., Heitto, A., Lopez-Hilfiker, F. D., Lutz, A., Riipinen, I., Hong, J., Donahue, N. M., Hallquist, M., Petäjä, T., Kulmala, M., and Yli-Juuti, T.: Molecular identification of organic vapors driving atmospheric nanoparticle growth, Nature Communications, 10, 10.1038/s41467-019-12473-2, 2019.